Journal of Ceramic Processing Research. Vol. 25, No. 2, pp. 268~277 (2024)
(Received 18 January 2024, Received in revised form 5 March 2024, Accepted 19 March 2024)
https://doi.org/10.36410/jcpr.2024.25.2.268

J O U R N A L O F
Ceramic Processing Research

Study on crystallization kinetics and curing mechanism of the multiple heavy metals in slag glass-ceramics

Yongsheng Du[a,*], Ying Wei[a], Zhicheng Zheng[a], Yuhang Guo[a], Hongxia Zhang[a], Leibo Deng[a], Hua Chen[a] and Ming Zhao[b]

[a]*College of Science, Inner Mongolia University of Science and Technology, Baotou 014010, China*
[b]*School of Material and Metallurgy (School of Rare Earth), Inner Mongolia University of Science and Technology, Baotou, 014010, China*

In this paper, manganese-containing blast furnace slag (MBFS) was used as the main raw material and Cr2O3 was used as the nucleating agent to prepare MBFS glass-ceramic by melting method. The influence of multiple heavy metal ions on the crystallization characteristics, physical and chemical properties of glass-ceramic was studied by adding CuO and ZnO, and the existence of multiple heavy metal ions in glass-ceramic and its curing effect were determined. The results showed that Cr was the key element for crystallization of glass-ceramic, which can enable volume crystallization to occur. The glass-ceramics with diopside as the main crystalline phase had excellent comprehensive physical and chemical properties. The results of TCLP heavy metal leaching experiments also confirmed that spinel crystal wrapped by diopside and glass phase can produce an excellent solidification effect on multiple heavy metals.

Keywords: MBFS, Glass-ceramic, Multiple heavy metal ions, Solidification.

Introduction

In the steel industry, blast furnace iron-making is a predominant technology, accounting for 95% of the world's total output of steel. The discharge of solid waste is significantly high, and blast furnace slag (BFS) is one of them. Many problems have been caused to the environment and ecological system owing to the exposure and accumulation of a large amount of BFS [1-3]. For example, the manganese-containing blast furnace slag (MBFS) in Baotou, Inner Mongolia, is the slag discharged from the blast furnace smelting with Bayan Obo iron ore (a typical co-associated polymetallic ore) as the main raw material. Continuous emissions of MBFS in the last 50 years have resulted in the formation of large-scale BFS mountain, which contains multiple kinds of heavy metals (Mn, Fe, Cu, Ti, Cr, rare earths) that may diffuse into water or soil, accumulate in organisms under enrichment, and may be transmitted to humans through the food chain, posing a certain threat to the ecological environment [4-7]. Therefore, the harmless treatment of the above BFS is an important issue that needs to be solved urgently. At present, the recovery of valuable metals, the tailings/slag backfilling or the use of tailings/slag for the production of construction materials such as concrete and cement are considered to be the full utilization of the BFS [8-10]. Among them, glass-ceramics prepared from BFS has excellent comprehensive performance and can be widely used as a structural or architectural decorative materials [11-14]. Meanwhile, the glass-ceramics can also effectively solidify the heavy metals in tailing/slag, which can achieve a high value, high efficiency and environmentally friendly use of solid waste. For example, Huang et al. used titanium-containing BFS and ferrochrome slag as the main raw materials to prepare glass-ceramics with augite as the main crystalline phase by melting method. When the content of BFS and ferrochrome slag were 36.89 and 27.67 wt%, respectively, the glass-ceramics had excellent comprehensive physical and chemical properties, with a flexural strength of 173.5 MPa and a hardness of 727.3 Hv [15]. Wang et al. successfully produced slag glass-ceramics with a maximum flexural strength of 194.5 MPa, acid resistance of 97.63% and Vickers hardness of 8.6 GPa using BFS as the main raw material by the melting method [16]. At the same time, the leaching concentration of the heavy metals Cr and Mn in the glass-ceramics was much lower than the leaching limits specified in the National Hazardous Waste Identification Standard (GB/T5085.3-2007), indicating that the glass-ceramics has better curing characteristics for the above heavy metals.

Determining the mechanism of curing heavy metals in glass-ceramics is the key to improve the curing effect. And the existence form of heavy metals in glass-ceramics has important guiding significance for revealing the

*Corresponding author:
Tel : +86-472-5954358
Fax: +86-472-5954358
E-mail: dys1111@imust.edu.cn

curing mechanism. Zou et al. prepared glass-ceramics from pure chemical reagents and simulated the migration and solidification characteristics of non-volatile and volatile heavy metals in tailings glass-ceramics by adding heavy metals Fe and Pb. The glass-ceramics effectively prevented the leaching of heavy metals through the double barrier effect of the crystalline and glass phase. The leaching concentrations of heavy metals Fe and Pb in the experiments were between 0.055 mg/L-0.087 mg/L and 0.074 mg/L-0.140 mg/L, which were far below the leaching standard threshold of US-EPA toxicity characteristic leaching procedure (TCLP) [17]. The glass-ceramics produced from waste incineration fly ash, waste glass and lead-zinc tailings as the main raw materials contained multiple kinds of heavy metal elements (Fe, Cu, Zn, Pb). Related experimental results showed that Fe was mainly present in the magnetite crystalline phase, Cu and Zn can enter into the magnetite lattice through isomorphic substitution, while Pb was solidified in the glass matrix in the form of ions. The order of the solidification effect of glass-ceramics on these four heavy metals was Fe > Zn > Cu > Pb [18]. Furthermore, heavy metal ions in glass-ceramics may also serve as nucleation agents, which can promote the nucleation and crystallization of glass-ceramics. For example, in the quaternary system CaO-MgO-Al_2O_3-SiO_2 (CMAS) glass–ceramics, chromium ions can greatly promote the precipitation of the main crystal phase of augite by forming spinel nuclei [19]. Thus, determining the existence characteristics and curing mechanism of multiple heavy metal elements in tailings/slag glass-ceramics can provide important theoretical guidance for the preparation of glass-ceramics with high corrosion resistance and low leachability.

Based on the above analysis, this paper takes MBFS as the main raw material for the preparation of glass-ceramics. Since Cr, Cu and Zn are the more common heavy metals found in various industrial solid wastes, it is necessary to conduct relevant studies on the curing properties of Cr, Cu and Zn in the glass–ceramics. By adding appropriate amounts of Cr_2O_3, CuO and ZnO, the presence and influence of multiple heavy metals on the microstructure, crystallography and nucleation mechanism of glass-ceramics are investigated. Through leaching experiments, heavy metal ions Cu, Zn, Cr and Mn in MBFS glass-ceramics are revealed [20]. The above study can provide important theoretical support for the preparation of BFS glass-ceramics with low leaching degree of heavy metals and excellent physical and chemical properties.

Experiments

Sample preparation

In this study, glass-ceramics were prepared from MBFS as the main raw material, in which the main compositions of MBFS were shown in Table 1. According to the phase diagram of CMAS system, the base glass composition was chosen as 46.65-49.28%SiO_2, 22.01-23.25%CaO, 8.68-9.15%MgO and 7.28-7.68%Al_2O_3 (wt.%) and the main crystalline phase of glass-ceramic was assigned as diopside. Table 2. presented the corresponding chemical composition of the investigated glass-ceramics. Among them, SiO_2 and MgO were added to make up for the glass base composition, and the addition of Na_2CO_3 was to reduce the glass melting temperature. In order to study the presence state of chromium, copper and zinc ions and their effects on the crystallization characteristics and properties of the glass-ceramics, Cr_2O_3, CuO and ZnO with different combination forms were added to the raw materials, and the corresponding sample numbers were Cu1, Zn2, CuZn3, Cr4, CrZn5, CrCu6 and CrCuZn7, respectively.

The prepared well-mixed samples were placed in a

Table 1. Chemical composition of MBFS (wt%).

Composition	SiO_2	CaO	MgO	Al_2O_3	K_2O	Na_2O	TFe	TiO_2	MnO	REO
wt%	34.60	36.79	9.57	12.16	0.48	0.74	0.5	0.34	0.75	4.07

Note: REO denotes the sum of rare earth oxides in the MBFS, including La_2O_3 (1.50 wt%) and CeO_2 (2.57 wt%).

Table 2. Ingredients of glass-ceramics (wt%).

Sample	BFS	SiO_2	Na_2CO_3	MgO	Cr_2O_3	CuO	ZnO
Cu1	63.19	27.42	3.69	3.11	/	2.59	/
Zn2	63.19	27.42	3.69	3.11	/	/	2.59
CuZn3	61.50	26.69	3.59	3.04	/	2.59	2.59
Cr4	63.19	27.42	3.69	3.11	2.59	/	/
CrZn5	61.50	26.69	3.59	3.04	2.59	/	2.59
CrCu6	61.50	26.69	3.59	3.04	2.59	2.59	/
CrCuZn7	59.84	25.95	3.49	2.95	2.59	2.59	2.59

muffle furnace, and heated from room temperature to 900 °C and held for two hours firstly, then continued to heat up to 1200 °C and kept for 3.5 hours, and finally heated to 1450 °C and held for three hours. Then, a small portion of the melts were poured directly into ice water to generate a water quenched sample, which were analyzed by differential scanning calorimetry (DSC). And the remaining melts were cast onto a preheated stainless steel mould and annealed in another resistance furnace at 600°C for 5 h. Finally, the slag glass-ceramics were obtained by a two-step heat treatment method according to the DSC results.

Characterization

The nucleation and crystallization temperatures of the glass-ceramics were determined by DSC (NETZSCH 449) at a heating rate of 10 ºC/min from room temperature to 1200 ºC at nitrogen atmosphere apparatus using α-alumina as reference. The Raman spectra of the parent glass samples using Raman spectrometer inVia in the range of 200-1200 cm^{-1} with excitation light source of 532 nm, is used for analyzing glass network structure and chemical bands. After heat treatment, the samples were ground into powders and passed through a 200 mesh sieve, and the crystalline phases of glass-ceramics were analyzed by powder X-ray diffraction (XRD, PANalytical) at room temperature in the range of 10º to 80º. XRD patterns were recorded using CuKα radiation with the work voltage of 40 KV, current of 40 mA, and scanning speed of 3°/min. Field emission scanning electron microscope (FESEM, Supra55, ZEISS) equipped with an Oxford energy dispersive spectrometer (EDS) were used to investigate the morphology and chemical composition of polished crystallized glass-ceramics. The leaching characteristic of heavy metals in glass-ceramics was determined using the Toxicity Characteristic Leaching Procedure (TCLP) according to the US EPA standards (US EPA 1311) [21, 22]. Firstly, the glass-ceramics samples were crushed so that the particles size could pass through a 9.5 mm aperture sieve. The polished samples were mixed with the acetic acid buffer solution (pH of 4.93±0.05) in the ratio of 1:20 (kg/L) and shaken at 30±2 rpm for 20 h at room temperature. Then an inductively coupled plasma spectrometer (ICP, Agilent Technologies 5110) was used to detect the leaching concentrations of heavy metals in the leaching agents. Measurements of microhardness of glass-ceramics were carried out using a Vickers hardness tester (HV-50A), and six indentation experiments were performed to obtain the average value. The bulk density of the glass-ceramics was measured by the Archimedes method. According to the industry standard for glass-ceramics tubes (JC/T2283-2014) [23], acid resistance was assessed by measuring the mass of glass-ceramics particles with a particle size of 0.5-1.0 mm before and after corrosion in a 20 wt% H_2SO_4 solution under the heating condition of a water bath at 100 ºC.

Results and Discussion

Thermal behavior analysis

The DSC curves of base glasses with different heavy metals addition are shown in Fig. 1 and 2, respectively, where the prepared base glasses in Fig. 1 have no Cr_2O_3 addition and the prepared base glasses in Fig. 2 contain a certain amount of Cr_2O_3. The glass transition temperature (T_g) and crystallization exothermic peak temperature (T_p) are clearly observed. Comparison shows that the intensity of the exothermic peak in Fig. 2 is overall higher than that in Fig. 1, which indicates that the addition of Cr_2O_3 helps to improve the crystallization characteristics of glass-ceramics [24]. It is also found in Fig. 2 that the T_p of the base glass is shifted toward higher temperature with the addition of ZnO, whilst the T_p of the base glass is shifted toward lower temperature with the addition of CuO. Generally speaking, zinc ion belongs to the intermediate oxides, which can play the role of supplementing the glass network structure as well as the role of breaking the [Si-O] net structure [25]. In

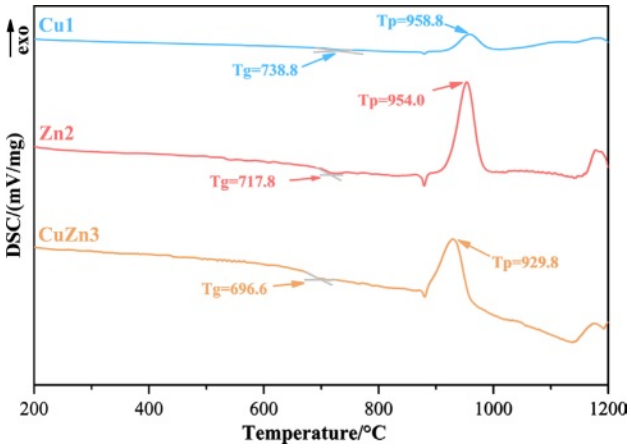

Fig. 1. DSC curves of the prepared base glasses without addition of Cr_2O_3.

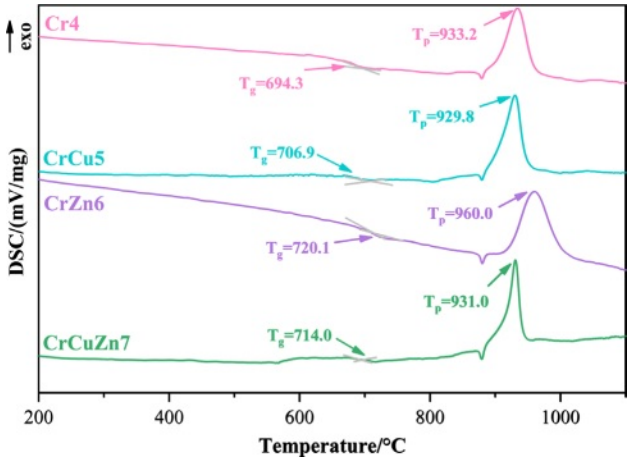

Fig. 2. DSC curves of the prepared base glasses with addition of Cr_2O_3.

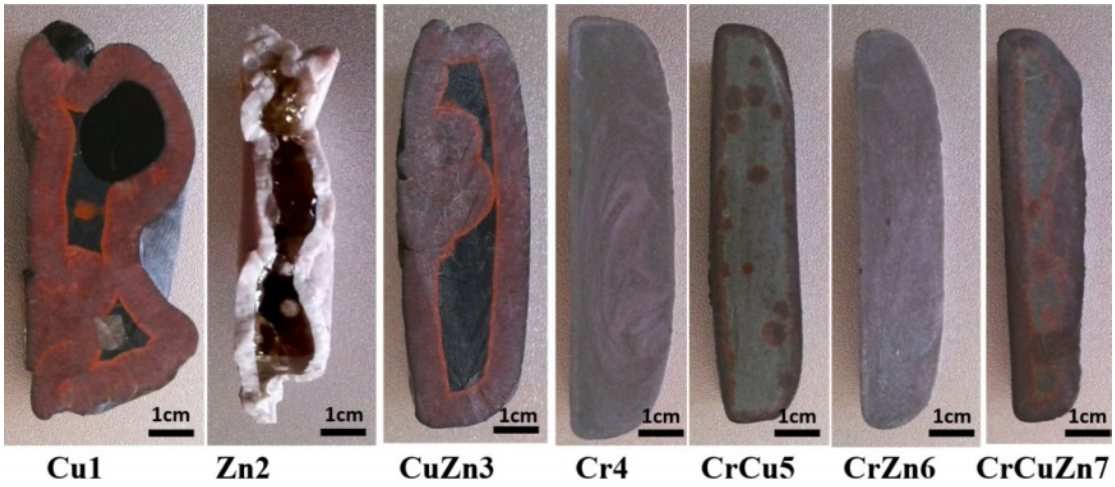

Fig. 3. Cross-sections of glass-ceramics with different heavy metals addition.

this experiment, ZnO with a relatively lower addition mainly has an aggregation effect on the glass network and enhances the glass network stability, which results in a rightward shift of the T_p. Instead, copper ion can act as the modifier for the glass network, which can break the [Si-O] or $[Al-O]^-$ network structure and reduce the polymerization level of the glass network [26, 27]. As a result, the crystallization ability of glass-ceramic can be improved. Moreover, it is also worth noting that the heat treatment temperature of glass-ceramic can be determined by the results of DSC [28]. The nucleation temperature is chose as 750 °C and the crystallization temperature is selected as 980 °C in this experiment.

Cross sectional photograph of crystallized glass-ceramics

According to the heat treatment temperatures determined from the DSC results, a two-stage heat treatment process is carried out on the base glasses, and the cross-sections of the crystallized glass-ceramics are shown in Fig. 3. A surface crystallization phenomenon can be found in the glass-ceramics without addition of Cr_2O_3 and the glass phase can be clearly observed in the enter section of the samples. Obviously, the samples with surface crystallization exhibit varying degrees of deformation or hollow phenomenon, which may lead to poor performance of the crystallized glass-ceramics. Conversely, Glass-ceramics containing Cr_2O_3 are fully crystalized as a whole, which suggests that chromium ions can be used as an effective nucleating agent to promote the crystallization of glass-ceramics. Some results also confirm that the chromium ions in glass-ceramics tend to form spinel nuclei, and the main crystalline phase of glass-ceramics can grow at the interface of spinel nuclei in the form of dendrite. Considering the crystallographic relation between spinel and diopside, it is probably $[001]_{diopside}//[112]_{spinel}$ [29]. Thus, diopside can grow epitaxially along the normal direction of the spinel, which contributes to the formation of interlocking crystalline phase. That is, the proper amount of Cr_2O_3 can strongly promote the bulk crystallization of glass-ceramics with an integrated interlocking crystal structure and may achieve the desired crystallization characteristics and properties.

In addition, it is found that the glass-ceramics containing CuO shows a copper-red color, which is apparently related to the color development mechanism of copper ions in glass-ceramics. Our related research results show that Cu^+ and Cu^{2+} are two main valence states of copper ions in glass-ceramics, and Cu^+ exists in glass-ceramics in the form of the cuprite phase (Cu_2O). The main reason for the appearance of copper-red color in glass-ceramics is the precipitation of cuprite crystals [30].

Structure evolution of base glasses

Since the network structure of the base glass is one of the important factors affecting the phase transition, Raman spectroscopy is used to investigate the influence law of different heavy metals addition on the network structure of the glass. Raman spectra of base glasses with various heavy metal addition are shown in Fig. 4(a). In general, the bands within the 800-1200 cm^{-1} range in the Raman spectra are mostly composed of antisymmetric stretching vibrations of bridging oxygen (BO) and non-bridging oxygen (NBO) [31-33]. As the basic glass network structure is generally constituted of $[SiO_4]$ tetrahedra, the structural units consist of $[SiO_4]^{4-}$ (monomer, 4 NBO atoms), $[Si_2O_7]^{6-}$ (dimer, 3 NBO atoms), $[Si_2O_6]^{4-}$ (cyclic chain, 2 NBO atoms), $[Si_2O_5]^{2-}$ (lamellar, 1 NBO atom) and $[SiO_2]$ (shelf, 0 NBO atom). The degree of polymerization of a glass network is usually determined by the relative content of Q^n (n represents the amount of BO), e.g. Q^0, Q^1, Q^2, Q^3 correspond to $[SiO_4]^{4-}$, $[Si_2O_7]^{6-}$, $[Si_2O_6]^{4-}$, $[Si_2O_5]^{2-}$, respectively. It should be pointed out that the Q^4 is not discussed due to its quite low intensity [34]. Since Q^n is usually determined by its corresponding area integral in the Raman spectrum, the relative contents of Q^0 (in

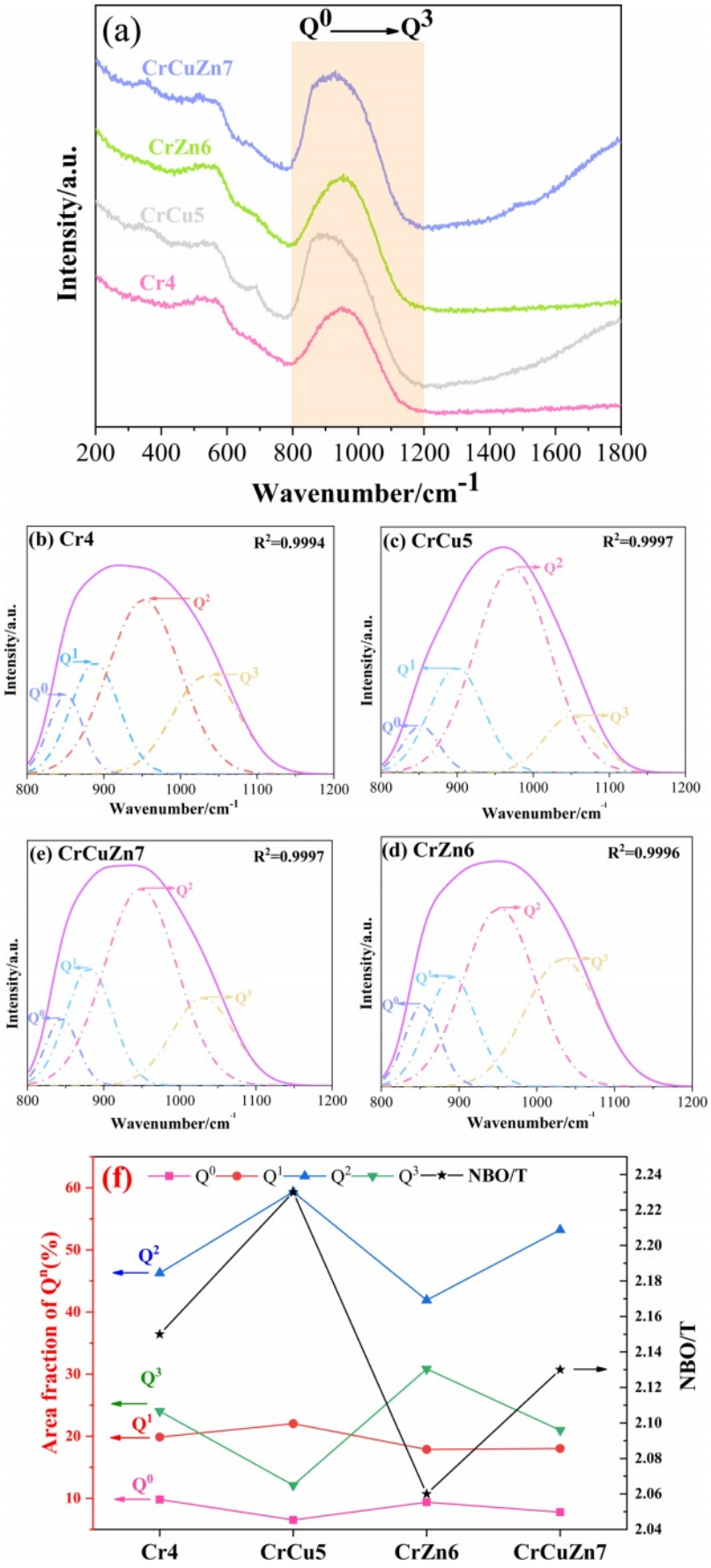

Fig. 4. Raman spectra and related deconvoluted results of base glasses: (a) Raman spectra of base glasses; (b) Cr4; (c) CrCu5; (d) CuZn6; (e) CuCuZn7; (f) structural unit proportion

Table 3. Q^n and NBO/T values in base glasses with different heavy metals addition.

Sample	Q^0	Q^1	Q^2	Q^3	NBO/T
Cr4	9.82	19.87	46.27	24.03	2.15
CrCu5	6.53	22.02	59.34	12.11	2.23
CrZn6	9.38	17.87	41.90	30.83	2.06
CrCuZn7	7.78	18.02	53.23	20.97	2.13

the range of 860-880 cm^{-1}), Q^1 (in the range of 920-935 cm^{-1}), Q^2 (in the range of 990-1000 cm^{-1}), and Q^3 (in the range of 1060-1070 cm^{-1}) can be analyzed using Gaussian peak differentiation, as shown in Fig. 4(b)-(e). Fig. 4(f) shows the relative fraction of Q^0, Q^1, Q^2, Q^3 and the ratio of NBO to total oxygen (NBO/T) in different base glasses, where NBO/T can be got by the following formula, and the corresponding results are also listed in Table 3.

$$NBO/T = 0\times Q^4 + 1\times Q^3 + 2\times Q^2 + 3\times Q^1 + 4\times Q^0 \quad (1)$$

Based on the analysis of the above data, the addition of CuO in glass-ceramic results in a significant increase in the degree of depolymerisation of the glass network and the value of NBO/T reaches a maximum. This is due to the fact that copper ions, as network modifier oxides, do not participate in the composition of the glass network and reduce the structural integrity of the glass network by breaking [Si-O] as well as the [Al-O] network structure [35]. In contrast, with the addition of ZnO, the value of NBO/T in base glass CrZn6 decreases significantly compared to that of Cr4, indicating that there is a tendency to decrease in the depolymerisation of the glass network, and therefore ZnO at this content plays a role in stabilising and compensating the glass network [36]. The above conclusion is consistent with the results of the DSC.

Phase formation

The XRD patterns of glass-ceramics with varying heavy metal contents are depicted in Fig. 5. It can be seen that the crystalline phases of the glass-ceramics comprise of diopside ($Ca(Mg,Al)(Si,Al)_2O_6$) and cuprite phase (Cu_2O). The precipitation of the main crystalline phase diopside is caused by the formation of spinel nuclei through the nucleating agent Cr_2O_3. The change of heavy metal species has no significant effect on the main crystalline phase of the glass-ceramics. However, the addition of CuO helps to produce a second phase of cuprite in glass-ceramics, and it can be explained that Cu^{2+} in the glass phase was reduced to Cu^+ under the action of high temperature [37]. Cu^+ gathered near the glass phase to form Cu_2O colloidal particles.

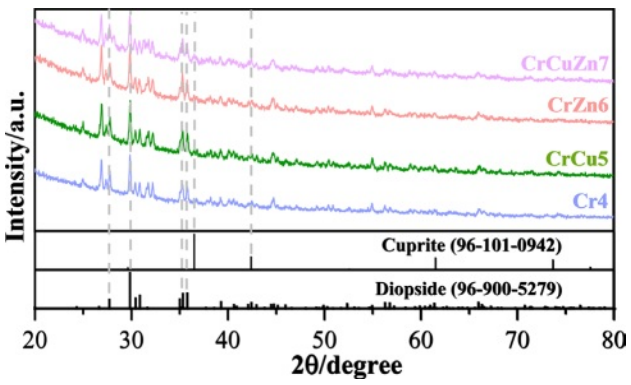

Fig. 5. XRD patterns of glass-ceramics with different heavy metals addition.

Surface morphology and element composition analysis

In order to determine the influence of heavy metals on the microstructure and element distribution of glass-ceramics, the surface morphology and element distribution of the polished glass-ceramics are characterized using FESEM and EDS element mapping, and the results are shown in Fig. 6. Combined with the results of XRD analyses, it can be determined that the Cr-rich region (region a) in glass-ceramics is spinel, and the Mg-rich region (region b) corresponds to the diopside phase. The spinel nucleus can act as a heterogeneous nucleation center and promote the formation of the diopside phase in the form of dendritic crystals. Based on the results from the Raman analysis, the crystallization degree of glass-ceramic is obviously improved with the addition of CuO. Accordingly, the crystal morphology is changed from dendrites to spherical crystals, as shown in sample CrCu5. Combined with the DSC and Raman results, the refinement in grain size can be explained as a depolymerization of silicon-oxygen network induced by copper ions. In addition, the EDS element mapping result also reveals that the Cu-rich region (region d) corresponds to the cuprite phase and the Al-rich region (region c) is the glass phase. It can be seen from the element distribution of crystal phases and glass phase in glass-ceramics that heavy metals Cu, Zn, Mn and Cr can be enriched in spinel crystals, indicating that these heavy metal elements can coexist stably in spinel crystals.

In order to accurately characterize the presence of heavy metals in the crystal phases and glass phase of glass-ceramics, EDS point scans are performed in all samples and the results are shown in Fig. 7. The regions (a), (b) and (c) correspond to the spinel phase, diopside phase and glass phase, respectively. The main elements in spinel are Cr, Mg, Al, Mn, Cu, Zn and O,

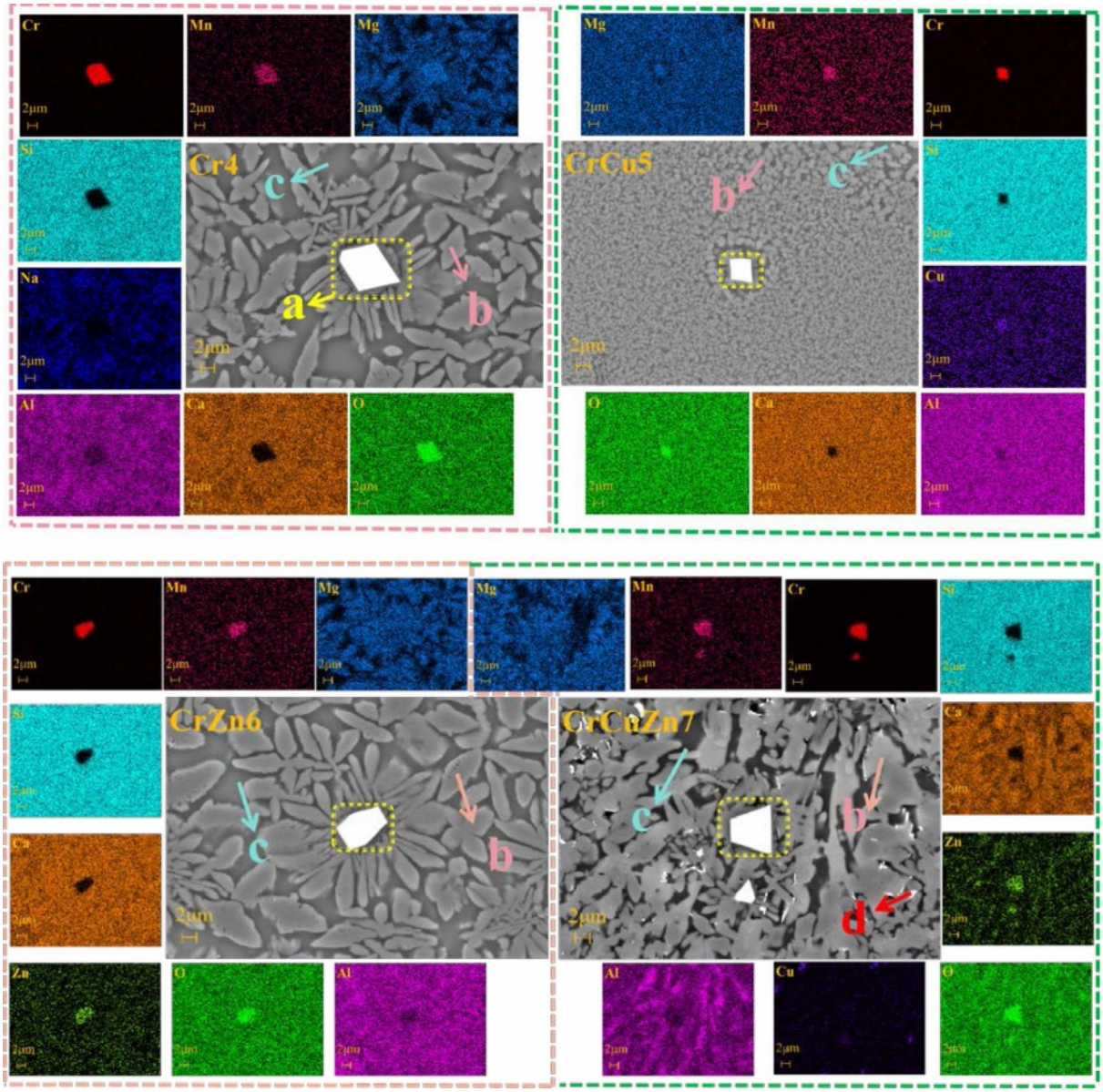

Fig. 6. FESEM and EDS element mapping of glass-ceramics with different heavy metals addition.

corresponding to the chemical formula (Mg, Mn, Cu, Zn)(Al, Cr)$_2$O$_4$. With the addition of the heavy metals CuO and ZnO, there is a significant tendency for the content of Mg^{2+} in spinel to decrease and the content of Cu^{2+} and Zn^{2+} to increase. The result indicates that Zn^{2+} and Cu^{2+} can enter into the lattice of spinel by replacing Mg^{2+}. The close proximity of the ionic radii contributes to the above substitution phenomenon among these ions [38], since the ionic radii of Mg^{2+}, Cu^{2+} and Zn^{2+} are 0.72, 0.73 and 0.74 Å, respectively. In diopside, it can be seen that the content of heavy metals Cr, Mn, Zn, Cu is relatively low and only a small amount of Cu^{2+} and Zn^{2+} can enter into the lattice of diopside by substituting for Mg^{2+}, which suggests that the diopside has a relatively stable structure, and the phenomenon of ion substitution is not obvious. For the glass phase, it contains extremely low heavy metals, and only a small amount of Cu^{2+} and Zn^{2+} can exist in the glass network.

Combined with the above analysis, a simulation diagram of heavy metal elements in crystal phases and glass phase is given in Fig. 8. In spinel, Mn^{2+}, Cu^{2+} and Zn^{2+} are generally located in the tetrahedral structure, and Cr^{3+} is found in the octahedral structure [39]. In diopside, Cu^{2+} and Zn^{2+} mostly occupy position X of diopside (XY(Si, Al)$_2$O$_6$) and Cr^{3+} is locate in the Y-site [40]. Compared with crystals, the presence of heavy metals in glass phase is more complex. Cu^{2+} predominantly presents in the form of octahedra, which present a depolymerization network in the glass network, reducing the viscosity of the glass and promoting crystallization. Zn^{2+} is more inclined to form a tetrahedral structure in glass network and enhances the glass network stability. In addition, it can be found that cuprite generally exists as colloidal particles in glass-ceramics.

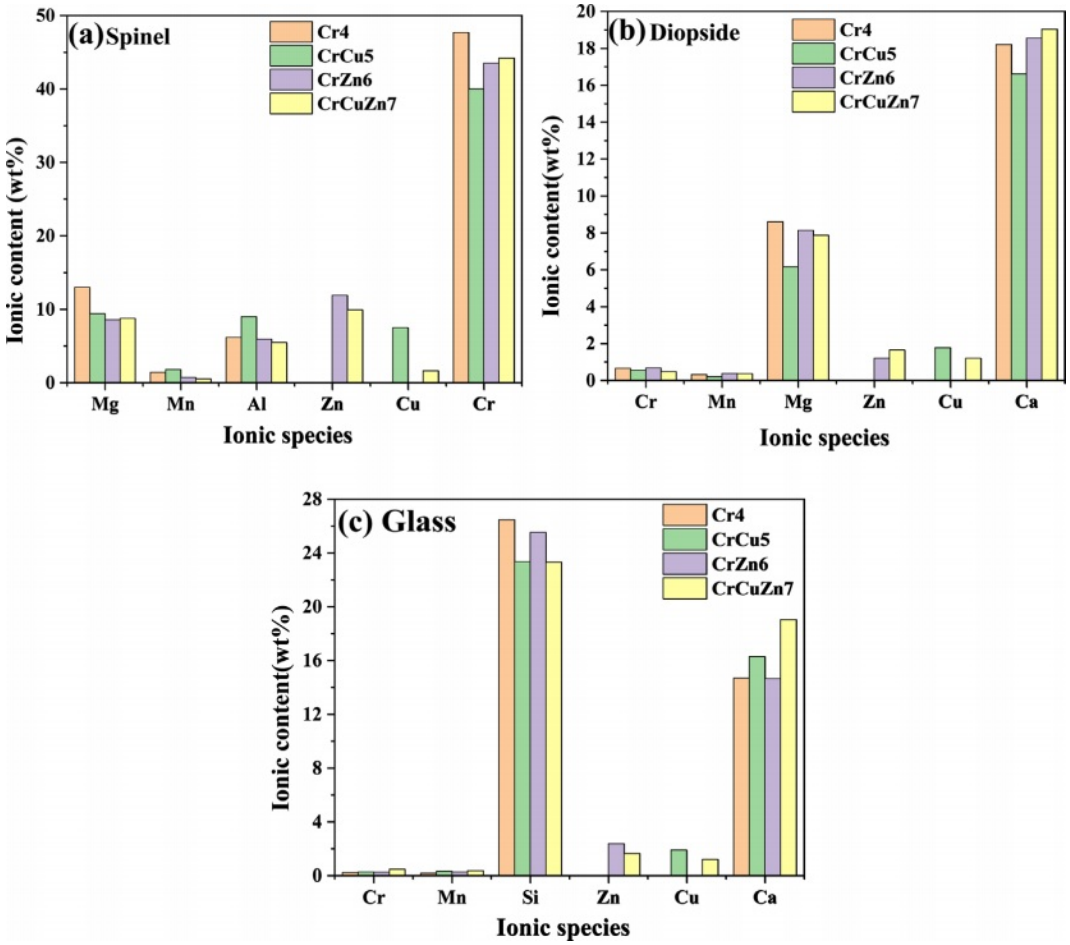

Fig. 7. EDS point scans of glass-ceramics with different heavy metals addition.

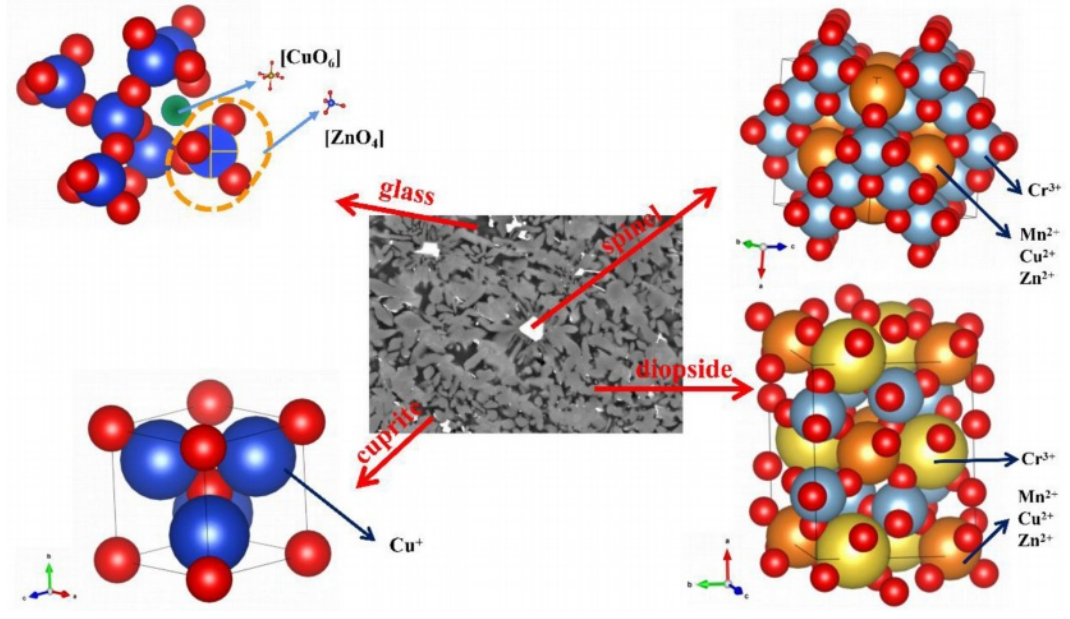

Fig. 8. Simulation diagram of heavy metal elements in crystal phases and glass phase.

Leaching properties of heavy metals

In order to determine the stability of heavy metals, such as Cu, Zn, Mn, Cr, in the prepared glass-ceramics, heavy metals leaching experimental studies are carried out according to TCLP standards, and the leaching concentrations of heavy metals are shown in Table 4. As

Table 4. Leaching test results of glass-ceramics with different heavy metals addition (mg/L).

Element	TCLP standard limits	Cr4	CrCu5	CrZn6	CrZnCu7
Cr	5	0.036	0.042	0.038	0.041
Mn	5	0.057	0.072	0.068	0.075
Cu	100	/	1.106	/	0.961
Zn	100	/	/	0.939	0.577

Table 5. Physicochemical properties of glass-ceramics with different heavy metals addition.

Sample	Cr4	CrCu5	CrZn6	CrCuZn7
Density (g/cm^3)	2.98	3.00	2.96	3.08
acid-resistant (%)	96.43%	92.23%	95.13%	93.63%
Vickers hardness (GPa)	8.54	8.64	8.51	8.57

can be seen from the table, the leaching concentration of heavy metal ions Mn and Cr in glass-ceramics is much lower than that of Cu and Zn, which is mainly due to the fact that Mn and Cr ions are mainly distributed in spinel. The results also confirm that spinel crystal wrapped by diopside and glass phase can produce an excellent solidification effect on heavy metals. While Cu and Zn ions, in addition to their distribution in the crystals, are also present in the glass phase or in the second phase of cuprite, and the stability of their existence is lower than that of Mn and Cr ions due to the fact that glass phase and Cu_2O colloidal particles are relatively easier to dislodge when the glass-ceramics are corroded by acetic acid buffer solution. In conclusion, heavy metals in glass-ceramics are mostly concentrated in the spinel, whilst the diopside phase grows in dependence on the spinel and plays a protective role for the spinel crystals, and the glass phase outside the crystal phase plays a protective role for the crystal phase. This synergistic mechanism of mutual protection can effectively solidify heavy metal ions such as Cu, Zn, Mn, Cr, etc., and the leaching concentrations of the corresponding heavy metal ions in glass-ceramics are all far below the standard values.

Physicochemical properties

The physical and chemical properties of glass-ceramics with different heavy metals addition are listed in Table 5. Amongst them, the acid resistance of the glass-ceramics is decreased with the addition of CuO. This may be due to the fact that some copper ions are present in the form of cuprite. The acid resistance of the cuprite phase is lower than that of the spinel and diopside phases, which leads to a decrease in the acid resistance of the Cu-containing glass-ceramics samples [41]. The leaching concentration of copper ions in heavy metal leaching experiment is greater than that of other heavy metal ions, which is also consistent with this conclusion. The density and Vickers hardness of the Cu-containing glass-ceramics is slightly higher than that of the other glass-ceramics. This is primarily due to the fact that Cu doping is helpful for grain refinement and the crystal morphology of glass-ceramic is changed from dendrites to spherical crystals with the addition of CuO. Grain refinement is helpful to increase in the uniformity of grain size distribution and enhance the compactness of glass-ceramics. Therefore, the density and Vickers hardness of glass-ceramics increase correspondingly. With the addition of ZnO, the Vickers hardness of the glass-ceramics is slightly lower than that of other glass-ceramics due to the fact that at this content ZnO mainly plays the role of a compensating the glass network, inhibiting the precipitation of glass-ceramics. Therefore, the Vickers hardness of glass-ceramics decreases accordingly. Comprehensive analysis shows that the glass-ceramics as a whole have excellent physicochemical properties. This is mainly due to the fact that the glass-ceramics with diopside as the main crystalline phase have excellent physical and chemical properties [42]. In addition, the high crystallinity degree and low defectivity of glass-ceramics are also one of the reasons for the excellent physical and chemical properties of glass-ceramics.

Conclusions

In this paper, high-performance glass-ceramics with low leaching rates were successfully prepared by using MBFS as main raw material. The existent state and leaching characteristic of multiple heavy metal ions in glass-ceramics were discussed. The following conclusions were obtained:

1. Glass-ceramics containing Cr_2O_3 were fully crystalized as a whole, while a surface crystallization phenomenon can be found in the glass-ceramics with addition of CuO or ZnO. The glass-ceramics with bulk crystallization had excellent comprehensive physical and chemical properties.

2. The presence of heavy metals in the crystal phases and glass phase of glass-ceramics can be accurately characterized. In spinel, Mn^{2+}, Cu^{2+} and Zn^{2+} are generally located in the tetrahedral structure, and Cr^{3+}

is found in the octahedral structure. In diopside, only a small amount of Cu^{2+} and Zn^{2+} can enter into the lattice by substituting for Mg^{2+}. Cu^{2+} and Zn^{2+} are present in glass network in the form of octahedral and tetrahedral, which mainly play a role in breaking the network and enhances the glass network, respectively.

3. MBFS glass-ceramics provide suitable matrixes for solidifying heavy metals and can simultaneously immobilize a wide range of heavy metal ions Cr, Mn, Cu and Zn. This study provides important theoretical support for the synergistic curing of multiple heavy metals.

Acknowledgments

This work was supported by National Natural Science Foundation of China (grant number 52060021), Natural Science Foundation of Inner Mongolia Autonomous Region (grant number 2023MS05035), Graduate Research Innovation Project of Inner Mongolia Autonomous Region, and Fundamental Research Funds for Inner Mongolia University of Science & Technology (2023QNJS121).

References

1. W.C. Xu, Z. Chao, R. Ma, N.N. Wu, and S.L. OuYang, J. Ceram. Process. Res. 24[3] (2023) 512-524.
2. Z.F. Tong, C.C. Xu, J.X. Wang, and Z.H. Jia, J. Ceram. Process. Res. 24[1] (2023) 17-28.
3. J.Y. Shi, J.X. Tan, B.J. Liu, J.Z. Chen, J.D. Dai, and Z.H. He, J. Hazard, Mater. 403 (2021) 123983.
4. G.Y. Wang, J. Ma, M. Zhao, S.L. Ouyang, L.B. Deng, H. Chen, and Y.S. Du, J. Ceram. Process. Res. 22[6] (2021) 665-674.
5. B.W. Li, Y.S. Du, X.F. Zhang, X.L. Jia, M. Zhao, and H. Chen, J. Ceram. Process. Res. 15[5] (2014) 325-330.
6. H.X. Zhang, Y.S. Du, X.W. Yang, S.L. OuYang, and B.W. Li, J. Ceram. Process. Res. 18[8] (2017) 604-610.
7. Y.S. Du, J. Ma, X.F. Zhang, H.X. Zhang, H. Chen, S.L. OuYang, and B.W. Li, J. Ceram. Process. Res. 20[4] (2019) 401-410.
8. Y.S. Du, X.W. Yang, H.X. Zhang, X.F. Zhang, M. Zhao, H. Chen, S.L. OuYang, and B.W. Li, Ceram. J. Ceram. Process. Res. 17[12] (2016) 1243-1248.
9. J. IwoNa and Gr. BaRtŁoMIeJ, Gospod. Surowcami Miner. - Miner. Resour. Manag. 38[4] (2023) 153-172.
10. A. Mahmood, M.T. Noman, M. Pechočiaková, N. Amor, M. Petrů, M. Abdelkader, J. Militký, S. Sozcu, and S.Z.U. Hassan, Polymers 13[13] (2021) 2099.
11. W.J. Duan, D.G. Wang, Z.M. Wang, Y.Q. Zhan, T.T. Mu, and Q.B. Yu, J. Clean. Prod. 329 (2021) 129804.
12. X. Liu, B. Li, and Y. Wu, J. Clean. Prod. 404 (2023) 136930.
13. K.Y. Chen, Y. Li, X.Y. Meng, L. Meng, and Z.C. Guo, Ceram. Int. 45 (2019) 24236-24243.
14. Y.L. Luo, F. Wang, H.Z. Zhu, Q.L. Liao, Y.L. Xu, and L.B. Liu, J. Non-Cryst. Solids 582 (2022) 121463.
15. R. Wang, X.F. Huang, S.C. Deng, W. Zhao, H.W. Guo, B.J. Yan, and P.J. Li, J. Non-Cryst. Solids 605 (2023) 122162.
16. X.F. Huang, W. Zhao, H.W. Guo, B.J. Yan, P. Li, and C.H. Li, Ceram. Int. 49 (2023) 9708-9718.
17. G.Y. Wang, Y.S. Du, Y.H. Guo, H.X. Zang, L.B. Deng, H. Chen, and M. Zhao, Environ. Prog. Sustain. Energy 42 (2023) 14019.
18. W.T. Zou, W.H. Zhang, Y.L. Pi, Y.S. Zhang, L. Zhang, and Y. Chen, Ceram. Int. 48 (2022) 5040-5053.
19. W.T. Zou, W.H. Zhang, Y.L. Pi, Y.S. Zhang, Y. Chen, and L. Zhang, Ceram. Int. 48 (2022) 36166-36177.
20. L.B. Deng, R.D. Jia, F. Yun, X.F. Zhang, H. Li, M.X. Zhang, X.L. Jia, D. Ren, and B.W. Li, Mater. Chem. Phys. 240 (2020) 122212.
21. W.P. Chen, R.Z. Jia, Y.X. Zhang, S.L. Ouyang, and N.N. Wu, J. Ceram. Soc. Jpn. 130 (2022) 376-383.
22. R.L. Zheng, J.F. Lyu, W.F. Song, M.D. Liu, H.S. Li, Y.L. Liu, X.J. Lyu, and Z.Y. Ma, Sep. Purif. Technol. 308 (2023) 122985.
23. L.B. Deng, Z. Fu, M.X. Zhang, H. Li, B. Yao, J.L. He, H. Chen, and Y. Ma, J. Non-Cryst. Solids 575 (2022) 121217.
24. J.F. Yu, Z.W. Peng, W.X. Shang, Q.X. Chen, G.Y. Zhu, H.M. Tang, M.J. Rao, and G.H. Li, Ceram. Int. 49 (2023) 15947-15958.
25. Y.S. Du, Y.H. Guo, G.Y. Wang, H.X. Zhang, L.B. Deng, H. Chen, and M. Zhao, J. Mater. Cycles Waste Manag. 25 (2023) 3081-3092.
26. M. Rao, S. Suresh, T. Narendrudu, A. Kumar, G. Ram, and D. Rao, J. Mol. Struct. 1125 (2016) 624-632.
27. M.A. Taha, R.A. Youness, G.T. El-Bassyouni, and M.A. Azooz, Silicon 13[9] (2021) 3075-3084.
28. J. Ma, Y. Shi, H. Zhang, S.L. Ouyang, L.B. Deng, H. Chen, M. Zhao, and Y.S. Du, Mater. Chem. Phys. 261 (2021) 124213.
29. Y.S. Du, M. Jie, Y. Ma, X.F. Zhang, H.X. Zhang, H. Chen, S.L. Ouyang, and B.W. L, J. Non-Cryst. Solids. 532[27] (2020) 119880.
30. Y.H. Guo, Y.S. Du, G.Y. Wang, Y. Xu, H.X. Zhang, L.B. Deng, H. Chen, and M. Zhao, Int. J. Appl. Ceram. Technol. 21 (2024) 796-805.
31. B. Zhang, Feng, He, X.H. Cao, M.J. Wei, C.C. Zheng, J. L. Xie, Ceram. Int. 48 (2022) 7013-7023.
32. Y.X. Zhang, H.R. Li, S.Y. Liu, N.N. Wu, and S.L. OuYang, J. Non-Cryst. Solids 563 (2021) 120701.
33. R.D. Jia, L.B. Deng, F. Yun, H. Li, X.F. Zhang, and X.L. Jia, Mater. Chem. Phys. 233 (2019) 155-162.
34. L.M. Chen, Y.L. Zhen, G.H. Zhang, L. Wang, D. Chen, H. Zhao, Y. Liu, F. Meng, Y. Peng, and T. Qi, J. Non-Cryst. Solids 602 (2023) 122080.
35. J.W. Xue, J.W. Zhong, Y.R. Mao, C.H. Xu, W. Liu, and Y.Q. Huang, Ceram. Int. 46 (2020) 23186-23193.
36. Y. Fan, F. He, Z. Li, W. Zhang, and J. Xie, Ceram-Silikaty 65[4] (2021) 334-343.
37. Y. Wang, Y. Wang, Y. Zhang, Y. Chai, F. Zhao, and G. Luo, Crystals 12 (2022) 1714.
38. R. Stefan, M. Karabulut, A. Popa, E. Culea, L. Bolundut, L. Olar, and P. Pascuta, J. Non-Cryst. Solids 498 (2018) 430-436.
39. S.C. Deng, C.R. Li, H.W. Guo, W. Zhao, B.J. Yan, and P. Li, J. Hazard. Mater. 445 (2023) 130621.
40. S.Z. Zhao, Q. Wen, X.Y. Zhang, B. Liu, and S.G. Zhang, Ceram. Int. 47 (2021) 21599-21609.
41. Y. Tang, Z.X. Fang, X.Y. Bai, Y.S. Du, H.X. Zhang, L.B. Deng, H. Chen, M. Zhao, X.D. Hao, and G.Y. Wang, J. Ceram. Process. Res. 24[1] (2023) 58-68.
42. D.F. He, C. Gao, J.T. Pan, and A.J. Xu, Ceram. Int. 44 (2018) 1384-1393.